Possible Cooperation of Differential Adhesion and Chemotaxis in Mound Formation of *Dictyostelium*

Yi Jiang,* Herbert Levine,# and James Glazier*

*Department of Physics, University of Notre Dame, Notre Dame, Indiana 46556; and #Department of Physics, University of California at San Diego, La Jolla, California 92093 USA

ABSTRACT In the mound stage of *Dictyostelium discoideum*, pre-stalk cells sort and form a tip at the apex. How this pattern forms is as yet unknown. A cellular level model allows us to simulate both differential cell adhesion and chemotaxis, to show that with differential adhesion only, pre-stalk cells move to the surface of the mound but form no tip. With chemotaxis driven by an outgoing circular wave only, a tip forms but contains both pre-stalk and pre-spore cells. Only for a narrow range of relative strengths between differential adhesion and chemotaxis can both mechanisms work in concert to form a tip containing only pre-stalk cells. The simulations provide a method to determine the processes necessary for patterning and suggest a series of further experiments.

INTRODUCTION

Dictyostelium discoideum is a classic model for biological pattern formation. Its life cycle shows a transition from solitary amoebas that aggregate to form a multicellular fruiting body. Aggregation is now understood in detail, both at the biochemical level and at the behavioral level. Propagating waves of cyclic adenosine monophosphate (cAMP) serve as the chemotactic signals which control collective cell motion. Aggregation leads to the formation of a multicellular mound, a hemispherical structure surrounded by a noncellular sheath, in which cells differentiate without spatial patterning into two major types (pre-stalk and pre-spore) (Williams, 1991; Loomis, 1995). Subsequently, the randomly distributed pre-stalk cells sort to the top of the aggregate to form a cylindrical nipplelike tip. This tip controls all morphogenetic movements during later multicellular development until the formation of the fruiting body (Rubin and Robertson, 1975).

How do the cells sort in the mound? Two possible mechanisms could govern relative cell motion: differential adhesion, in which differences in contact energy at cell interfaces bias the direction of cell motion, and chemotactic motion of cells along a chemical gradient. The former results from the local interaction between individual cells while the latter depends on diffusion of chemical signals over longer distances.

Under the differential adhesion hypothesis (Steinberg, 1963), the bonding strength between two cells depends on the types of cells involved, where the affinity of cell adhesion molecules on the cell membranes determines the adhesion energy. Additional energy comes from the surface tension between cells and the extracellular medium. These energetics bias the otherwise random movement of cells in aggregates, causing them to rearrange into patterns with minimal surface energy. Examples of such patterns in 2D can be seen in Glazier and Graner (1993). Research based on sorting in chicken embryo cells shows that many types of cells perform a biased random walk, with diffusion caused by cytoskeletally driven membrane fluctuations (Mombach and Glazier, 1996). Such differential adhesion-driven aggregates are usually convex in shape, since a quasi-ellipsoidal shape minimizes total surface area, and thus total surface energy.

In chemotaxis, a diffusible chemical, such as cAMP or NH_3, serves as a signal that instructs cells to move along the local chemical gradient toward higher or lower chemical concentrations. During aggregation, some cells spontaneously emit cAMP, initiating an excitation wave that propagates outward as a concentric ring or a spiral wave, as the signal is relayed by the surrounding cells (Caterina and Devreotes, 1991). Individual cells respond to a temporal and/or spatial increase of cAMP and start pulsatile chemotactic movement in the direction of higher cAMP concentration (Varnum et al., 1986; Wessels et al., 1992). Unlike differential adhesion, chemotactic cell motion is highly organized over a length scale significantly larger than the size of a single cell.

While intercellular adhesion is essential for *Dictyostelium* in the transition from unicellular amoebas to the multicellular stage (Bozzaro and Ponte, 1995; Levine et al., 1997), its direct involvement in the cell sorting in the mound is unclear. Conceivably, intercellular adhesion only passively keeps cells together while diffusible signals morphoregulate. Alternatively, adhesive energy differences might drive the cell motion while diffusible chemical gradients might be absent or merely enhance the process, or proper tip formation may require the collaboration of both mechanisms. To study these issues, we model cell sorting in the mound using a cell level cellular automaton, with dynamics based on

Received for publication 26 January 1998 and in final form 10 August 1998.

Address reprint requests to Dr. Yi Jiang, CNLS MSB258, Los Alamos National Laboratory, Los Alamos, NM 87545. Tel.: 505-665-7816; Fax: 505-665-2659; E-mail: yi@cnls.lanl.gov.

Herbert Levine's E-mail address is levine@herbie.ucsd.edu.

James Glazier's E-mail address is jglazier@rameau.phys.nd.edu.

0006-3495/98/12/2615/11 $2.00

experimental results concerning differential adhesion and chemotaxis in the life cycle of *Dictyostelium*.

The molecular basis of intercellular adhesion just before and during aggregation has been studied intensively. The csA glycoprotein in particular, which mediates adhesion during aggregation, is one of the best defined cell adhesion molecules (Bozzaro and Ponte, 1995). However, the cell surface components mediating cell adhesion during the mound and slug stages and the potential role of cell adhesion in tip formation and morphogenesis have not received as much attention, because of the inherent complexity of the multicellular stages. In addition, the prevailing notion is that pattern formation and morphogenetic movements in *Dictyostelium* depend mostly on diffusible chemical signals (for example, Traynor et al., 1992; Siegert and Weijer, 1995); although how the purported signaling center becomes established at the top of the mound is obscure.

Some evidence suggests that pre-stalk and pre-spore cells have different homotypic adhesivity. Tipped aggregates are more difficult to dissociate with EDTA than aggregation stage cells. When slugs form, pre-spore cells are much more resistant to EDTA dissociation than pre-stalk cells (Lam et al., 1981), and in an aggregate with mixed pre-stalk and pre-spore cells, pre-stalk cells move to the outer periphery of the aggregate (Siu et al., 1983). These results strongly suggest that pre-spore cells are more cohesive than pre-stalk cells. However, other lines of evidence point to the opposite conclusion, namely that pre-stalk cells are more cohesive than pre-spore cells (Tasaka and Takeuchi, 1981; Takeuchi et al., 1988; Traynor et al., 1994). The work of Takeuchi et al. (1988) even suggested that the slime sheath may help pre-stalk cells to come to the surface of the aggregate.

Chemotaxis may play a significant role in the sorting, since *Dictyostelium* cells can certainly respond chemotactically to chemical gradients. However, because of the difficulty of directly imaging chemical fields, no definitive evidence supports this possibility. Instead, one typically resorts to inferences from other more easily observed phenomena. Dark-field imaging attempts to visualize chemical waves using the changes in light scattering of cells during chemotactic cell movement. This technique works well during aggregation, but poorly in the mound. Only recently has the mound been visualized using dark-field images, showing that the waves propagate as concentric rings, spirals, or multiarmed spirals depending on the strain and experimental conditions (Siegert and Weijer, 1995); however, it is far from obvious how to associate 3D distributions of putative chemical signals with the dark-field images. Time-lapse movies based on fluorescent labeling have shown rotational cell movement in mounds of the wild-type strain AX-3 (Siegert and Weijer, 1995), and measurements of single cell velocity and changes in cell shape and trajectories show that cells move faster in the mound than during aggregation (Rietdorf et al., 1996). The McNally group, using time-lapse 3D optical-sectioning microscopy, examined the distribution of movement in mounds of AX-2 (Doolittle et al., 1995); they found no large-scale rotation, and cells moved in a variety of trajectories in the mound. While the pre-stalk cells moved ~50% faster than pre-spore cells, their migration paths were indistinguishable; in the KAX-3 strain, pre-stalk cells moved to the surface of the mound but often did not form a tip (Kellerman and McNally, private communication).

As already mentioned, much current thinking assumes that the dark-field waves in the mound are related to cAMP waves (as they are during aggregation) and that the measured motion is dominated by cAMP chemotaxis. One attempt to study the role of cAMP in cell sorting in the mound involved controlling the concentration of cAMP via the over-expression of secreted phosphodiesterase in the mound. It was observed that no tip formed with the over-expression, and this was interpreted to mean that the cAMP level was too low to properly guide cells (Traynor et al., 1992); furthermore, exogenous cAMP could make pre-stalk cells go to the mound base, also suggesting that chemotaxis to cAMP determines tip formation. Supporting evidence comes from the finding that a mutant strain having a deletion of a pre-stalk specific low-affinity cAMP receptor (CAR2) cannot form tips (Saxe et al., 1993). The idea that the cAMP wave detection by the cells switches from the usual high-affinity receptor (CAR1) to one with lower affinity is consistent with the phenomenology seen via the dark-field technique (Vasiev et al., 1997), if one makes the crucial assumption that these waves are related to cAMP. However, a recent report shows that *Dictyostelium* development is independent of cAMP as long as the catalytic subunit of cAMP-dependent protein kinase is present (Wang and Kuspa, 1997). In the acaA$^-$; act15:pkaC mutant, *Dictyostelium* development seems "near-normal" without detectable accumulation of cAMP, suggesting that signals other than extracellular cAMP can coordinate morphogenesis in *Dictyostelium*. If sorting and tip formation in the mound can occur at normal rates and without any undue sensitivities, cAMP may not be essential to these processes. Since our simulation applies equally to any chemoattractant, these findings do not affect our result, as long as chemotaxis to some chemical exists. Here we do not investigate other possibilities, such as a chemorepellent or a more complicated interaction with the slime sheath or the extracellular matrix.

MODEL

Our cellular automaton model (Graner and Glazier, 1992; Glazier and Graner, 1993) is based on a series of simplifications of the biology. First, we assume that all cells have differentiated to either pre-stalk cells (20% by volume) or pre-spore cells (80%). The cells have fixed surface properties that do not change during sorting and their volumes are constrained to be more or less constant. Second, the surface properties of cells are isotropic. Real *Dictyostelium* cells undergo elongation and contraction during aggregation as well as during mound formation (Rietdorf et al., 1996). We

neglect cell polarity or membrane curvature dependence. Hence, cells adhere with an energy per unit contact area that depends on the cell types involved. Third, as we do not explicitly consider extracellular matrix in the mound, cells interact with their neighbors through direct contact. We assume a layer of sheath, which may have different contact energy with different cell types, has formed around the mound before we start our simulations.

In our lattice model, each lattice site contains a number, σ, corresponding to the unique index of a cell. The domain of sites with the same index belongs to the same cell having type τ and volume v, and the differences of indices describe the membrane surfaces, as shown schematically in Fig. 1. Adhesive energy resides on the membrane surfaces only, while cells have no internal boundary energy. The sheath around the mound and the substrate supporting the mound are also represented as generalized "cells," but with particular properties and different surface tensions. To keep the aggregate from falling apart, we choose the surface tensions such that cells are more adhesive to each other than to substrate or to sheath. As the cells do not grow or shrink during sorting, we set a target volume V_σ for both pre-spore and pre-stalk cells. Deviation from the target volumes increases the total energy and is not favored. A similar model described the morphological changes of *Dictyostelium* from aggregation to migrating slug, but did not include cell sorting (Savill and Hogeweg, 1997).

In highly damped motions such as cell movement, motion stops as soon as the applied force stops. The velocity, rather than the acceleration, is proportional to the applied force, or $u \propto F$. For cells that move chemotactically, a reasonable hypothesis is that the cell velocity satisfies $u \propto \nabla C$, where C is the local chemical concentration. Since (in general) force is proportional to the gradient of the potential energy, we can treat chemotaxis as derived from an effective potential energy, although of course the chemoattractant does not directly exert a force on the cells. We also assume that cells rectify traveling wave signals to move only opposite to the direction of wave propagation (Goldstein, 1995), by making the chemotactic response vanish when the cells are in their (chemical) refractory state.

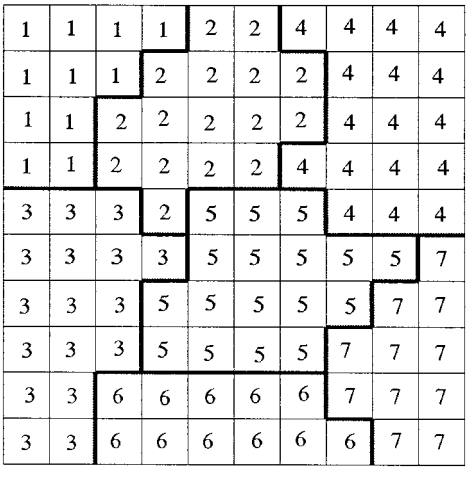

FIGURE 1 A 2D schematic of the model: an index at each lattice site, different indices indicate different cells, and the differences describe the membranes among them. Cells have different types τ and volumes v.

The total effective energy of the mound is

$$H = \sum_{\sigma} \sum_{\sigma'} J_{\tau(\sigma),\tau(\sigma')}(1 - \delta_{\sigma,\sigma'}) + \lambda \sum_{\sigma} [v_\sigma - V_\sigma]^2 + \sum_{i} \mu C_i(x, t), \quad (1)$$

where σ' is a neighbor of σ with the index σ ranging from 1 to N, the total number of cells. The coupling strength, $J_{\tau(\sigma),\tau(\sigma')}$, depends on the types of cells, $\tau(\sigma)$, involved. Larger $J_{\tau(\sigma),\tau(\sigma')}$ means more energy is associated with the interface between σ and σ', which is less energetically favorable, corresponding to weaker adhesivity. Surface tensions can be expressed in terms of the couplings between different cell types:

$$\gamma_{\tau,\tau'} = J_{\tau,\tau'} - \frac{J_{\tau,\tau} + J_{\tau',\tau'}}{2}, \quad (2)$$

$$\gamma_{\tau,M} = J_{\tau,M} - \frac{J_{\tau,\tau}}{2}, \quad (3)$$

where $\gamma_{\tau,\tau'}$ refers to the heterotypic surface tension of any pair of cell types, and M refers to the medium (sheath or substrate). These surface tensions, γ, are not equivalent to a biological membrane's internal tension, which appears instead as part of the membrane elasticity, λ. The γs represent the difference in energy between heterotypic and homotypic interface per unit area of membrane (Glazier and Graner, 1993), which are experimentally measurable (Foty et al., 1996). The second term in the total energy (Eq. 1) applies to the pre-stalk and pre-spore cells only, confining them near a fixed target volume V_σ so that they do not grow or shrink. The factor λ has units of energy per volume squared, corresponding to the elasticity of the cell membrane.

The last term is the effective chemical potential energy. $C_i(x,t)$ is the local concentration of the chemoattractant, which depends on time t and position x, and μ is the effective chemical potential. Physically, the gradient of a potential is force. The local chemical gradient effectively exerts a force on the part of the cell membrane that sees the gradient. If $\mu < 0$, the cell membrane protrudes pseudopodia toward higher chemical concentrations and cells move up the chemical gradient. If $\mu > 0$, cells move toward lower concentrations. Thus, μ corresponds to the cell motility, which converts a chemical gradient into a velocity. Cell motility has been studied extensively in *Dictyostelium*. Fisher et al. (1989) studied cell motility in a chemotaxis chamber which has stationary chemical gradients and found that the speed of AX-2 cells is 3 μm/min at a cAMP gradient of 25 nM/mm with midpoint 25 nM/mm. Soll et al. (1993) developed a 3D dynamic image analyzing system that produces detailed information about cell motility and

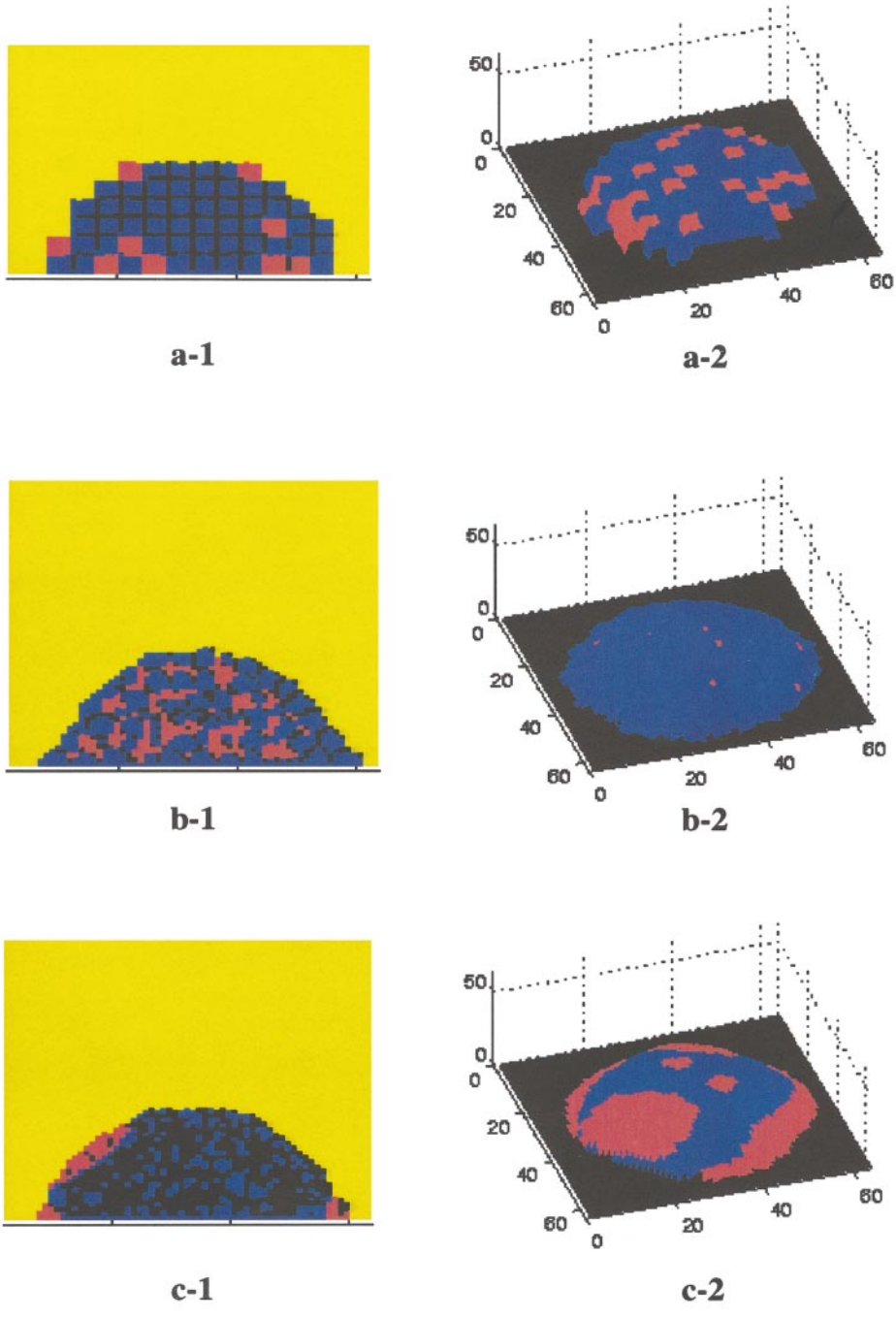

FIGURE 2 Sorting with differential adhesion only. (*a-1*) A vertical cross-section view of the mound at time 0. About 20% pre-stalk cells (red) randomly distributed among pre-spore cells (blue); cell surfaces are colored black. (*a-2*) A 3D surface plot of the mound at time 0. (*b*) A vertical section view and a surface plot of the mound with pre-stalk cells more cohesive than pre-spore cells, when both cell types have the same adhesivity with sheath ($J_{psp,psp} = 15$, $J_{pst,pst} = 5$, i.e., pre-stalk cells five times more cohesive than pre-spore cells, $J_{psp,sheath} = J_{pst,sheath} = 10$), at 20000 Monte Carlo steps (MCS). (*c*) same as (*b*) but with pre-stalk cells less cohesive than pre-spore cells ($J_{psp,psp} = 1$, $J_{pst,pst} = 3$, $J_{psp,sheath} = J_{pst,sheath} = 10$), at 6000 MCS. (*d*) A vertical section view and a surface plot of the mound with pre-stalk cells more adhesive to sheath than pre-spore cells ($J_{pst,sheath} = 10$, $J_{psp,sheath} = 25$, i.e., pre-stalk cells are 2.5 times more adhesive to sheath than pre-spore cells). Pre-stalk cells are more cohesive ($J_{psp,psp} = 15$, $J_{pst,pst} = 5$, i.e., pre-stalk cells are three times more cohesive than pre-spore cells), at 2000 MCS. Pre-stalk cells move to the surface of the mound, leaving some small clusters of pre-stalk cells in the bulk. (*e*) Same as (*d*) but with pre-spore cells more cohesive than pre-stalk cells ($J_{psp,psp} = 1.0$, $J_{pst,pst} = 3$, i.e., pre-spore cells are three times more cohesive than pre-stalk cells), at 200 MCS.

morphology based on the 3D paths of the centroid and the 3D contour of the cell. Their data show the cells moving at a velocity of 12–15 μm/min during natural aggregation, when the concentration of cAMP is rising from 10 to 1000 nM. We define the control parameter, the relative strength of chemotaxis and differential adhesion as

$$\phi = \mu/\gamma_{psp-pst}, \tag{4}$$

where $\gamma_{psp-pst} = J_{psp-pst} - (J_{psp} + J_{pst})/2$ is the heterotypic surface tension between pre-spore and pre-stalk cells. We can adjust ϕ to control the relative strength of chemotaxis and differential adhesion.

The pattern evolves by the standard Monte Carlo procedure, where an index at a cell-cell boundary is chosen at random and provisionally reassigned to one of its neighbor indices. The probability of accepting such a reassignment $\mathcal{P}$ is

$$\mathcal{P} = \begin{cases} 1 & \Delta H \le 0 \\ \exp(-\Delta H/T) & \Delta H > 0, \end{cases} \tag{5}$$

where ΔH is the change in effetive energy caused by the trial modification. T is a parameter that controls the amplitude of cytoskeletally driven membrane fluctuations, which

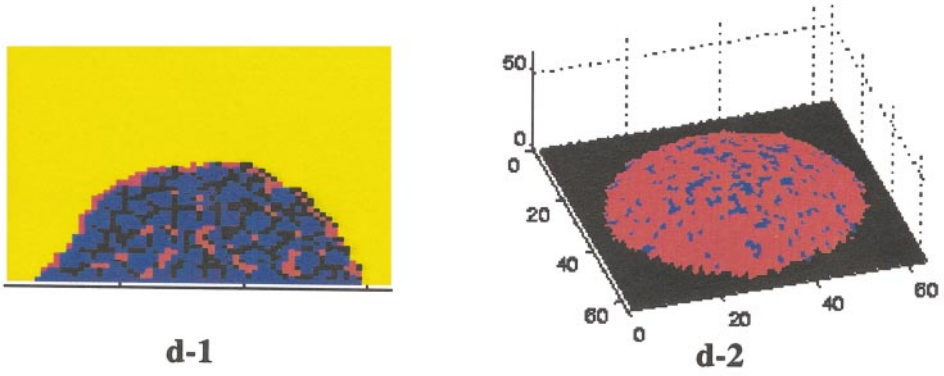

FIGURE 2 Continued.

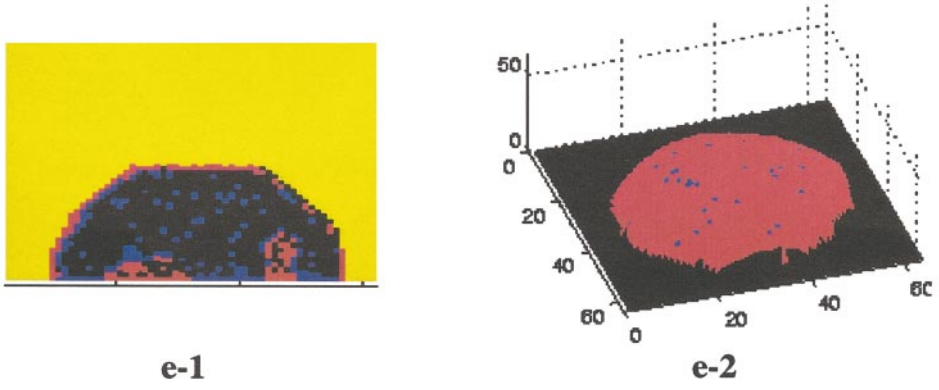

in turn determines the degree of sorting. Simulation time is measured by Monte Carlo steps (MCS). One MCS consists of as many trial lattice modifications as the total number of lattice sites.

We set the parameters $J_{pst,substrate} = J_{psp,substrate} = 20$ and the membrane elasticity $\lambda = 10$. Since the substrate does not participate in the index reassignment, the choice of $J_{cell,substrate}$ is only to set the surface tensions between cells and substrate for correct contact angles. The effect of λ on simulations has been studied by Glazier and Graner (1993). The behaviors of the cells are not sensitive to the exact value of λ ranging from 3 to 30. The value of λ is chosen such that the cells remain compact while keeping close to the target volume. Without chemical dynamics, the amplitude of membrane fluctuation observed for chicken embryo retinal cells is ~ 1 μm for cells with a diameter of 5–10 μm. We choose the amplitude of membrane fluctuation to be $T = 10$, which corresponds to a typical boundary fluctuation of one lattice site for a cell of size $4 \times 4 \times 4$ in the absence of chemotaxis.

In simulations that consider differential adhesion only, we set the chemical potential μ to zero, i.e., cells do not respond to chemical signals. Because of the confusion in the literature on the relative adhesivity of pre-spore and pre-stalk cells and the lack of current experimental data, we tried both possibilities: Figs. 2*b* and 2*d* show the simulation with pre-stalk cells more cohesive than pre-spore cells ($J_{psp,psp} = 15$, $J_{pst,pst} = 5$, i.e., pre-stalk cells are more cohesive than pre-spore cells, corresponding to $\gamma_{pst-sheath}$: $\gamma_{psp-sheath} = 0.38$), whereas Figs. 2*c* and 2*e* have the pre-spore cells more cohesive ($J_{psp,psp} = 1.0$, $J_{pst,pst} = 3.0$, corresponding to $\gamma_{pst-sheath}$:$\gamma_{psp-sheath} = 2.6$). Experiments measuring the surface tensions of chicken embryo tissues found γ_{liver}:γ_{heart} = 4.3 dyn/cm:8.3 dyn/cm = 0.52 (Foty et al., 1996). Our choices of surface tensions are biologically reasonable. We have also varied whether or not the pre-stalk cells have a preferential interaction with the sheath boundary, to see the extent to which this hypothesized mechanism might be necessary to reproduce experimental sorting patterns.

In accord with dark-field observations, we set up an artificial 2D chemical target pattern with a source located in the center column of the mound. The source radiates chemoattractant periodically outward at a constant speed, giving rise to a concentration field:

$$C_p(r, t) = C_{p0} \exp[\sin(r + \xi t) - 1]/r, \qquad (6)$$

in which r is the distance from a site to the center of the horizontal plane where the site is located, and ξ is the traveling velocity of the chemical wave. We recognize that the choice of chemical field is somewhat arbitrary, but it leads to waves consistent with the simplest interpretation of the circular dark-field waves seen in the AX-2 mound (Siegert and Weijer, 1995). We have obtained similar results using a 3D pacing wave emanating from the top of the

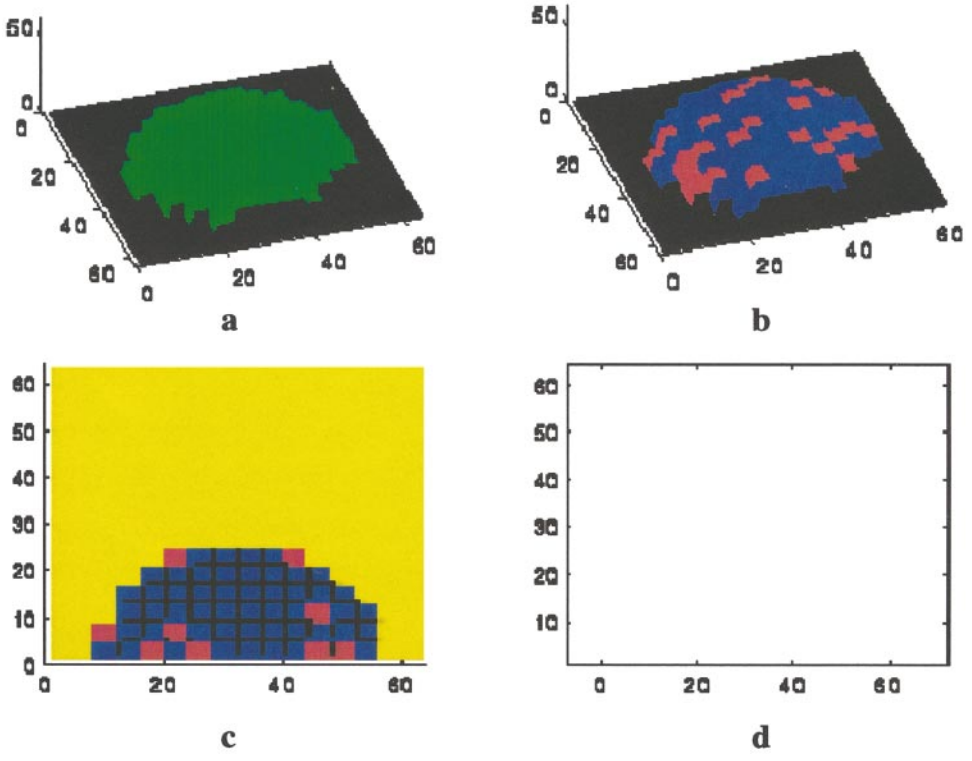

FIGURE 3 Initial configuration for simulations with both differential adhesion and chemotaxis. ($J_{psp,psp}$ = 1.0, $J_{pst,pst}$ = 3.0, μ = 20). (*a*) A 3D surface plot of the mound showing different states of the cells: green represents quiescent, purple active, and yellow refractory. (*b*) A 3D surface plot of the mound showing cell type distribution: pre-spore cells are shown blue and pre-stalk cells red. (*c*) A vertical cross-section of the mound showing cell type distribution: pre-spore cells are shown blue and pre-stalk cells red, cell surfaces black. (*d*) A projection, from the top, of the chemical concentration on the surface of the substrate. The chemical field is zero at time 0.

mound. We have also tried to replace this pacing wave with a single pacemaker cell on the top of the mound. Although waves will propagate throughout the mound from this cell, we have not yet found a consistent set of parameters that leads to tip formation. Essentially, waves that propagate are too "spiky" to elicit a strong chemotactic response, which requires a long-lived gradient. Inasmuch as no experimental data are available on the 3D distribution of chemoattractant

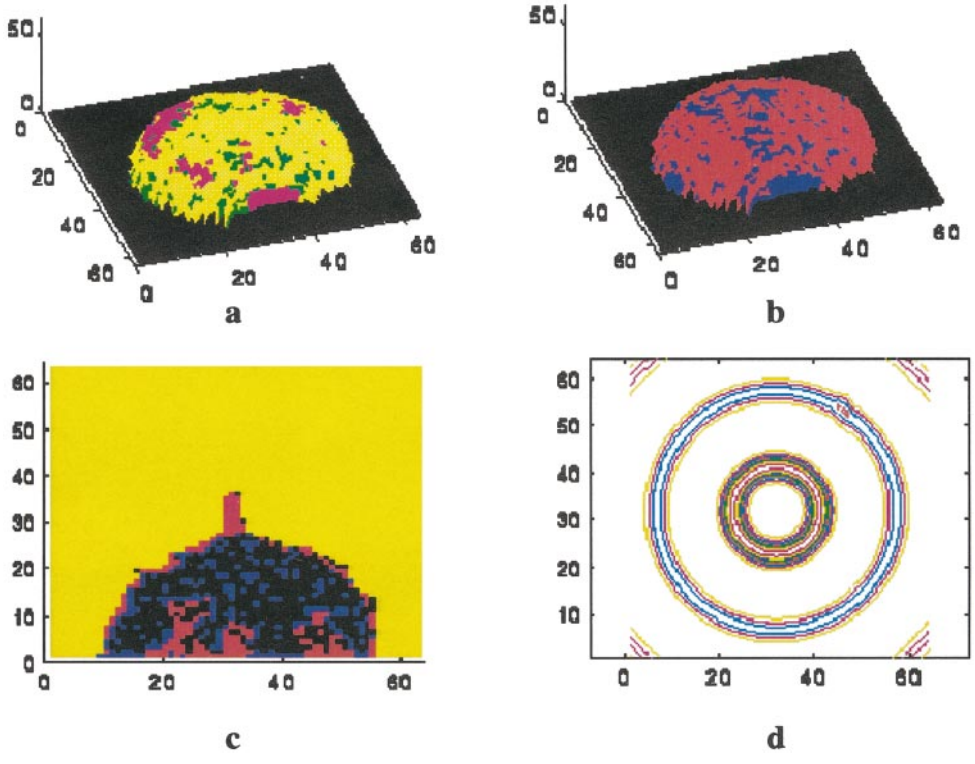

FIGURE 4 The same mound as in Fig. 3 at 2000 MCS for simulations with both differential adhesion and chemotaxis.

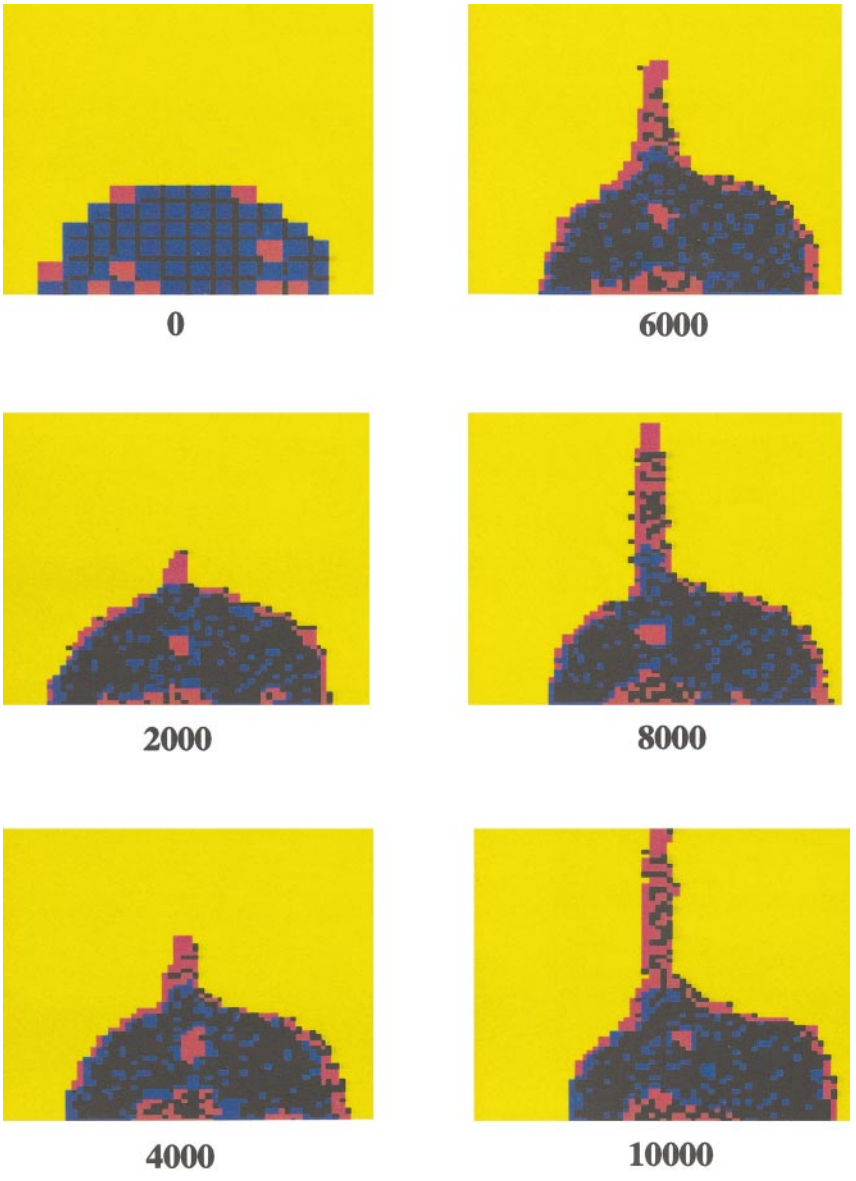

FIGURE 5 Vertical section views of the evolution of a mound ($J_{psp,psp} = 1$, $J_{pst,pst} = 3$, $\mu = 20$). Numbers show time in MCS.

in the mound, the pacing assumption is reasonable and simple (McNally, private communication).

We borrow the cell's chemical cycle from Kessler and Levine (1993) which successfully models aggregation. The cells may be quiescent, active, or refractory (an enforced recovery period following an active period). Once activated by a chemical signal (induced by a temporal chemical gradient above a threshold), cells secrete a fixed amount of the same chemical (relay) and can move chemotactically toward higher chemical concentration. The chemical also diffuses within the mound and on the surface of the substrate, decays due to proteolytic degradation (similar to that of cAMP by phosphodiesterase), and is secreted by the pacemaker and active cells. We can write the chemical dynamics as

$$\frac{\partial C}{\partial t} = D\nabla^2 C - \beta C + C_0 + C_p, \qquad (7)$$

where D is the diffusion constant and β is the rate of degradation. C_0 is the secretion by active cells and C_p is the autocatalytic pacing field given in Eq. 6. In all the simulations mentioned in this paper, we use the following parameters for the chemical dynamics: $D = 5$, $\beta = 0.5$, $C_0 = 50$, $C_p = 0.6$, and $\xi = 1.05$. Most of these values are from Kessler and Levine (1993).

We simulate pure chemotactic motion by letting the surface tensions for pre-spore and pre-stalk cells be the same, eliminating distinctions between the cell types.

Some experiments suggest that pre-stalk cells respond more strongly to cAMP than pre-spore cells (Sternfeld and David, 1981). Can differential chemotaxis to some agent play a significant role? We incorporated this possibility by letting μ have different values for different cell types. However, the simulation results were independent of this differential chemotactic response for relative μ differing up to 50% (data not shown). Therefore, the experimentally

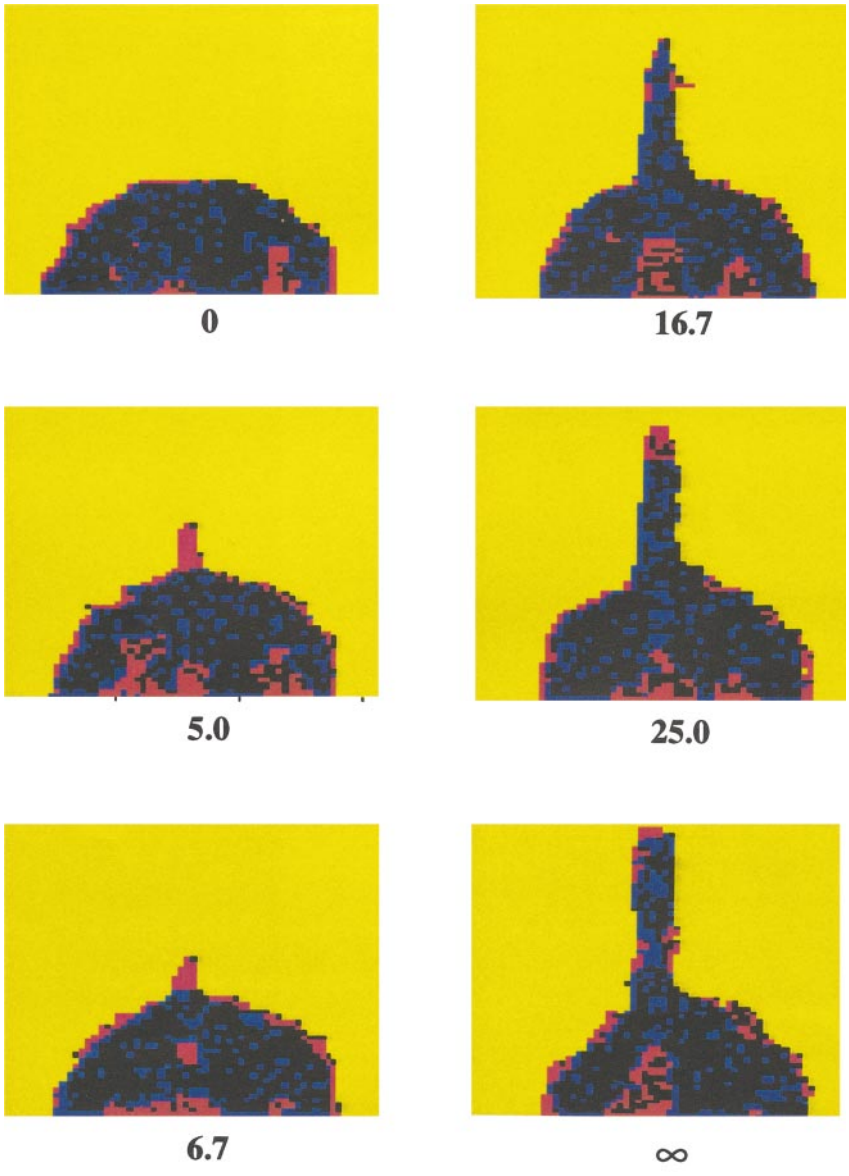

FIGURE 6 Vertical section views of the mounds at 2000 MCS for different relative strengths. Numbers show the values of the control parameter ϕ ($\phi = \infty$ corresponds to chemotaxis only, see text for description).

observed differences in cAMP response are probably not significant for cell sorting in the mound. In particular, they cannot explain the sorting of pre-stalk cells to the surface.

RESULTS

In the absence of chemotaxis

Fig. 2 *a-1* shows a vertical cross-section of the hemispherical mound at time 0, sitting on the substrate, surrounded by the slime sheath. Pre-stalk cells are red and pre-spore cells blue. Black represents the boundaries between cells (cell surface pixels). Fig. 2 *a-2* is the corresponding 3D surface view. The mound contains ~500 cells; 20% of them are pre-stalk cells, randomly distributed in the mound. If both cell types interact equally with sheath, the more cohesive cell type should form a cluster inside the other cell type. Fig. 2 *b* shows that when pre-stalk cells are more cohesive, they form clusters inside the pre-spore aggregate (derived from the decrease in contact areas between pre-spore and pre-stalk, data not shown). Fig. 2 *c* shows the opposite case when pre-spore cells are more cohesive: over time, pre-stalk cells are "squeezed" to the surface as the pre-spore cells cluster to form a single aggregate, with a few pre-stalk cells trapped inside. (Note that cells extend pseudopods when they move. Hence, their surface areas increase, increasing the number of black pixels in the cross-section views.) Therefore, sorting of pre-stalk cells to the surface does not require them to adhere more strongly to sheath, as long as pre-spore cells are more cohesive; the signature of more cohesive pre-stalk cells in experiment would be the occurrence of clusters of pre-stalk cells at the surface, which would not spread into a thin layer covering the whole mound. In neither case can a tip form.

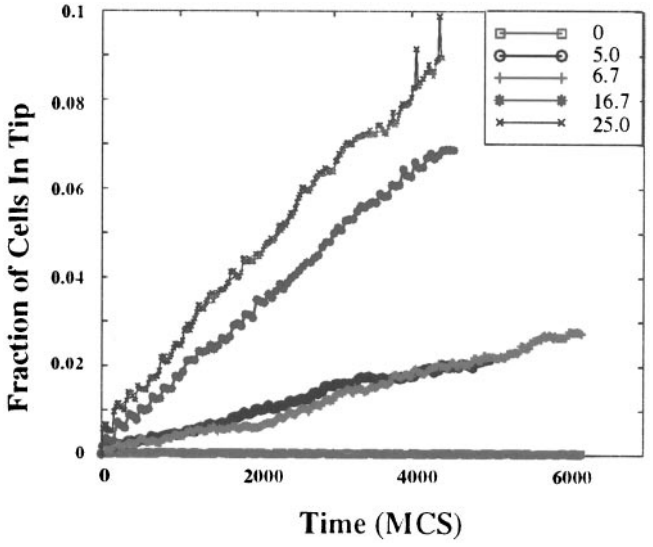

FIGURE 7 The evolution of tip size (fraction of cells in the tip) as a function of time for a series of ϕ.

But if pre-stalk cells adhere more strongly to sheath than pre-spore cells, as suggested in Takeuchi et al. (1988), pre-stalk cells would move to the surface of the mound to minimize the contact area between pre-spore cells and sheath, whether or not they are more cohesive than pre-spore cells. When we set pre-stalk cells to be more cohesive (shown in Fig. 2 *d* at 2000 MCS) pre-stalk cells move slowly to the surface of the mound, leaving some small pre-stalk clusters behind; no tip forms. If the pre-spore cells are more cohesive (shown in Fig. 2 *e* at 200 MCS), more pre-stalk cells appear on the surface, with some small clusters of pre-stalk cells left behind within the bulk of the mound; again, no tip forms. The only difference between the cases is that cells come to the surface more slowly for more cohesive pre-stalk cells, since they tend to cluster, and since cell motion is driven by membrane fluctuations, clusters diffuse more slowly than single cells. These possibilities could be distinguished experimentally by checking whether pre-stalk cells tend to form small clusters before they come to the surface.

In the results that follow, we assume that the true situation in *Dictyostelium* is the parameter set corresponding to Fig. 2 *e*. That is, we take pre-spore cells to be more cohesive and include some pre-stalk surface preference. These parameters lead to the most rapid and most robust (when varying the other parameters) sorting of the pre-stalk cells to the mound surface. Even in this case, though, no tip forms.

The patterns developed under differential adhesion in mutants that are likely to have chemotactic defects are similar to those seen in both carB (Saxe et al., 1993) and tagB (Shaulsky et al., 1995) null mutants. That is, pre-stalk cells form a thin surface layer on top of the mound but never form a protruding tip. If those mutants somehow interfere with the chemotactic system (either by deleting a relevant receptor or, for tagB, by eliminating a subclass of cells that may be involved in initiating the chemical signal), these findings would be consistent with our model dynamics.

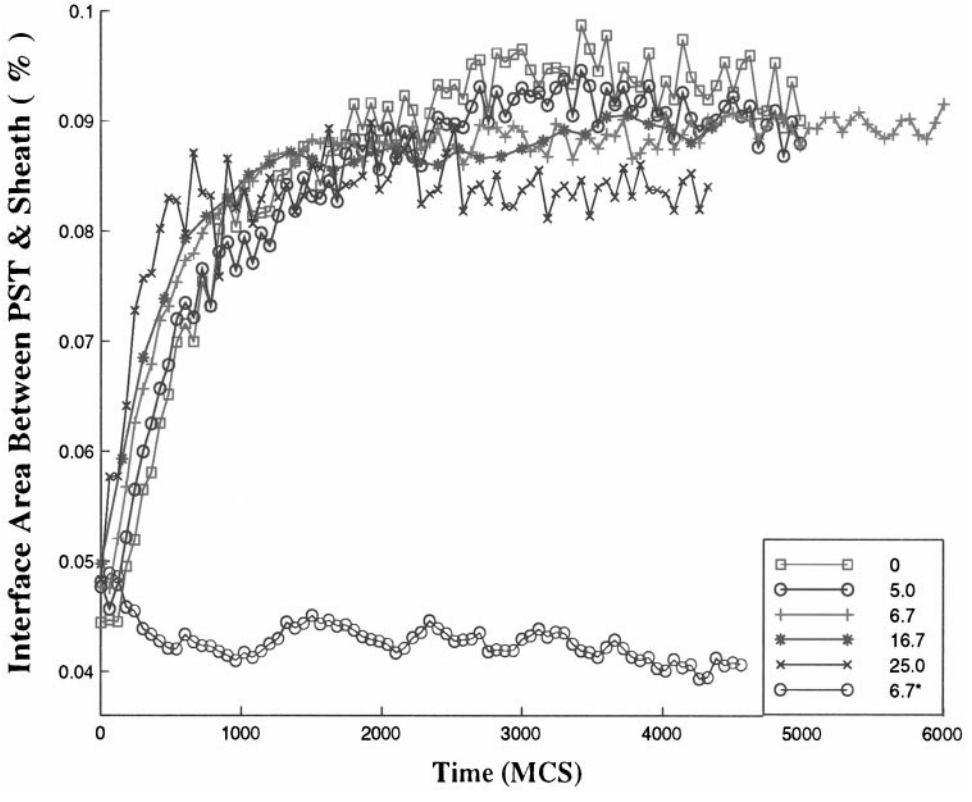

FIGURE 8 The fraction of pre-stalk cells in contact with the sheath as a function of time for a series of ϕ. ϕ = 6.7* corresponds to the case of pure chemotaxis, with pre-stalk and pre-spore cells having the same surface tensions.

With chemotaxis

When we include chemotaxis, an apical tip forms. Fig. 3 shows a typical initial condition for simulations with chemotaxis: *a* shows a 3D surface plot of the mound, and color codes indicate the different states of cells (green for quiescent, purple for active, and yellow for refractory). At time 0, all cells are quiescent (green); *b* shows the cell type distribution on the surface of the mound: blue represents pre-spore cells and red represents pre-stalk cells; *c* is a vertical cross-section through the mound; we can see red (pre-stalk) cells randomly distributed; black represents cell surface; *d* shows the chemical concentration (a view from the top) at the surface of the substrate, which is zero initially. Fig. 4 shows the pattern evolved after 2000 MCS. A tip begins forming at the apex of the mound and the pre-stalk cells move to the surface. Fig. 5 shows typical evolution in the mound with both mechanisms present. As time progresses, the tip grows taller and taller. Pre-stalk cells sort to the surface of the mound and, in particular, make up the majority of cells in the protruding tip. This sequence is consistent with observations in strains such as AX-2.

As we adjust ϕ to tune the relative strength of chemotaxis to differential adhesion, we see that the pattern formation results from the competition between the minimization of adhesion energy (differential adhesion) and cell movement toward higher chemical concentration (chemotaxis), shown in Fig. 6. Stronger chemotaxis produces a large tip more rapidly, but the tip contains both pre-stalk and pre-spore cells, with no sorting of cell types. Chemotaxis only, when pre-stalk and pre-spore cells have the same adhesion energy, corresponds to $\phi = \infty$. Only within a certain range ($5 < \phi < 8$) does a tip form containing pre-stalk cells only. For $\phi = 6.7$, the maximum velocity of cell motion is $\sim$1.5 lattice sites per MCS or 4 cell diameters per 10 MCS, measured from the center of the mass of cells. If we equate 20 MCS to 1 min in real time, the cell velocity corresponds to $\sim$16 μm/min, as observed experimentally (Soll et al., 1993). This timescale in turn makes the sorting time $\sim$100 min, which is realistic.

To provide experimentally verifiable quantitative results, we measured the size of the tip as a function of time for a series of relative strengths. Fig. 7 shows that all the tips grow linearly in time with larger chemical potential u corresponding to faster tip growth. Next, we measured the fraction of contacting surface between pre-stalk cells and sheath to indicate the degree of cell sorting to the surface. Shown in Fig. 8, larger chemical potential results in faster but less complete sorting. The asterisk ($\phi = 6.7$*) indicates the case of pure chemotaxis, i.e., with pre-spore and pre-stalk cells having the same surface tensions, when no sorting to the surface was observed. Notice that the slopes of the interface areas are steeper for larger ϕ before 1000 MCS, suggesting that at short times, at least, chemotaxis could enhance the speed of sorting. Again, the degree of surface sorting is easily measurable experimentally. Thus the experimentally determined rate of growth and degree of sorting will determine ϕ.

In conclusion, our simulation results suggest the following: 1) in the mound stage, if differential adhesion alone regulated cell sorting, pre-stalk cells would come to the surface of the mound but no tip would form. In other words, differential adhesion alone cannot explain the formation of a sorted tip. 2) Chemotaxis of cells to some diffusible chemical radiated from the mound center can result in tip formation, but the tip consists of both pre-stalk and pre-spore cells; no sorting can be accomplished by chemotaxis alone. 3) Only under the competition of both mechanisms can the cells move to form a tip consisting of pre-stalk cells only. Similar methods can be used to study strains such as KAX-3, which have been seen to have "pinwheel" waves, or to consider alternative mechanisms such as a chemorepellent emitted by the pre-spore cells. While the basic mutations of both AX-2 and KAX-3 have not been well characterized, our results suggest that the KAX-3 strain may be defective in chemotaxis, so that it often does not form tips.

Experiments measuring the cohesiveness of pre-stalk and pre-spore cells, and the interfacial tensions between pre-stalk/sheath and pre-spore/sheath, are called for to determine the crucial parameters. Further measurements of the tip growth rate and degree of surface sorting in wild-type *Dictyostelium* mound can determine the relative strength of differential adhesion and chemotaxis.

The authors thank Prof. W. Loomis as a constant source of information and constructive remarks and Prof. J. G. McNally for many illuminating discussions.

This work was supported in part by National Science Foundation Grants DMR-92-57001-006, INT 96-03035-0C (to Y.J. and J.A.G.), and DBI-95-12809 (to H.L.), and by ACS/PRF (to Y.J. and J.A.G.).

REFERENCES

Bozzaro, S., and E. Ponte. 1995. Cell adhesion in the life cycle of *Dictyostelium*. *Experientia.* 51:1175–1188.

Caterina, M. J., and P. M. Devreotes. 1991. Molecular insights into eukaryotic chemotaxis. *FASEB J.* 5:3078–3085.

Doolittle, K. W., I. Reddy, and J. G. McNally. 1995. 3-D analysis of cell movement during normal and myosin-II-null cell morphogenesis in *Dictyostelium*. *Dev. Biol.* 167:118–129.

Fisher, P. R., R. Merkl, and G. Gerisch. 1989. Quantitative analysis of cell motility and chemotaxis in *Dictyostelium discoideum* by using an image processing system and a novel chemotaxis chamber providing stationary chemical gradients. *J. Cell Biol.* 108:973–984.

Foty, R. A., C. M. Pfleger, G. Forgacs, and M. S. Steinberg. 1996. Surface tensions of embryonic tissues predict their mutual development behavior. *Development.* 122:1611–1620.

Glazier, J. A., and F. Graner. 1993. Simulation of the differential adhesion driven rearrangement of biological cells. *Phys. Rev. E.* 47:2128–2154.

Goldstein, R. E. 1995. Traveling-wave chemotaxis. *Phys. Rev. Lett.* 77: 775–778.

Graner, F., and J. A. Glazier. 1992. Simulation of biological cell sorting using a two-dimensional extended Potts model. *Phys. Rev. Lett.* 69: 2013–2016.

Kessler, D., and H. Levine. 1993. Pattern formation in *Dictyostelium* via the dynamics of cooperative biological entities. *Phys. Rev. E.* 48: 4801–4804.

Lam, T. Y., G. Pickering, J. Geltosky, and C. H. Siu. 1981. Differential cell cohesiveness expressed by prespore and pre-stalk cells of *Dictyostelium discoideum*. *Differentiation*. 20:22–28.

Levine, H., L. Tsimring, and D. Kessler. 1997. Computational modeling of mound development in *Dictyostelium*. *Physica D*. 106:375–388.

Loomis, W. F. 1995. Lateral inhibition and pattern formation in *Dictyostelium*. *Curr. Top. Dev. Biol.* 28:1–46.

Mombach, J. C. M., and J. A. Glazier. 1996. Single cell motion in aggregates of embryonic cells. *Phys. Rev. Lett.* 76:3032–3035.

Rietdorf, J., F. Siegert, and C. J. Weijer. 1996. Analysis of optical density wave propagation and cell movement during mound formation in *Dictyostelium discoideum*. *Dev. Biol.* 177:427–438.

Rubin, J., and A. Robertson. 1975. The tip of the *Dictyostelium discoideum* plasmodium as an organizer. *J. Embryol. Exp. Morphol.* 33:227–241.

Saxe, C. L. 3d, G. T. Ginsburg, J. M. Louis, R. Johnson, P. N. Devreotes, and A. R. Kimmel. 1993. CAR2, a prestalk cAMP receptor required for normal tip formation and late development of *Dictyostelium discoideum*. *Genes Dev.* 7:262–272.

Savill, N., and P. Hogeweg. 1997. Modeling morphogenesis: from single cells to crawling slugs. *J. Theor. Biol.* 184:229–235.

Shaulsky, G., A. Kuspa, and W. F. Loomis. 1995. A multidrug resistance transporter/serine protease gene is required for prestalk specialization in *Dictyostelium*. *Genes Dev.* 9:1111–1122.

Siegert, F., and C. J. Weijer. 1995. Spiral and concentric waves organize multicellular *Dictyostelium discoideum*. *Curr. Biol.* 5:937–943.

Siu, C., B. D. Roches, and T. Y. Lam. 1983. Involvement of a cell-surface glycoprotein in the cell-sorting process of *Dictyostelium discoideum*. *Proc. Natl. Acad. Sci. U.S.A.* 80:6596–6600.

Soll, D., D. Wessels, and A. Sylvester. 1993. The motile behavior of amoebae in the aggregation wave in *Dictyostelium discoideum*. *In* Experimental and Theoretical Advances in Biological Pattern Formation. H. G. Othmer, P. K. Maini, and J. D. Murrays, editors. Plenum Press, London. 325–338.

Steinberg, M. S. 1963. Reconstruction of tissues by dissociated cells. *Science*. 141:401–408.

Sternfeld, J., and C. N. David. 1981. Cell sorting during pattern formation in *Dictyostelium*. *Differentiation*. 20:10–21.

Takeuchi, I., T. Kakutani, and M. Tasaka. 1988. Cell behavior during formation of prestalk/prespore pattern in submerged agglomerates of *Dictyostelium discoideum*. *Dev. Genet.* 9:607–614.

Tasaka, M., and I. Takeuchi. 1981. Role of cell sorting in pattern formation in *Dictyostelium discoideum*. *Differentiation*. 18:191–196.

Traynor, D., R. H. Kessin, and J. G. Williams. 1992. Chemotactic sorting to cAMP in the multicellular stages of *Dictyostelium* development. *Proc. Natl. Acad. Sci. U.S.A.* 89:8303–8307.

Traynor, D., M. Rasaka, I. Rakeuchi, and J. Williams. 1994. Aberrant pattern formation in myosin heavy chain mutants of *Dictyostelium*. *Development*. 120:591–601.

Varnum, B., K. B. Edwards, and D. R. Soll. 1986. The developmental regulation of single-cell mobility in *Dictyostelium discoideum*. *Dev. Biol.* 113:218–227.

Vasiev, B., F. Siegert, and C. Weijer. 1997. Multiarmed spirals in excitable media. *Phys. Rev. Lett.* 78:2489–2492.

Wang, B., and A. Kuspa. 1997. *Dictyostelium* development in the absence of cAMP. *Science*. 277:251–254.

Wessels, D., J. Murray, and D. R. Soll. 1992. Behavior of *Dictyostelium* amoebae is regulated primarily by the temporal dynamics of the natural cAMP wave. *Cell Motil. Cytoskel.* 23:145–156.

Williams, J. G. 1991. Regulation of cellular differentiation during *Dictyostelium* morphogenesis. *Curr. Opin. Genet. Dev.* 1:338–362.